BASIC SCIENCE

Nanomedicine: Nanotechnology, Biology, and Medicine
11 (2015) 671–679

Original Article

nanomedjournal.com

Biodistribution and *in vivo* toxicity of aptamer-loaded gold nanostars

Duncan Hieu M. Dam[a,1], Kayla S.B. Culver[b,1], Irawati Kandela, PhD[c], Raymond C. Lee[a], Kavita Chandra[b], Hyojin Lee, PhD[a], Christine Mantis[c], Andrey Ugolkov, PhD[c], Andrew P. Mazar, PhD[c], Teri W. Odom, PhD[a,b,*]

[a]*Department of Chemistry, Northwestern University, Evanston, IL, USA*
[b]*Department of Materials Science and Engineering, Northwestern University, Evanston, IL, USA*
[c]*Developmental Therapeutic Core, Chemistry of Life Processes Institute, Northwestern University, Evanston, IL, USA*

Received 19 June 2014; accepted 18 October 2014

Abstract

This paper reports an *in vivo* evaluation of toxicology and biodistribution of a highly anisotropic Au nanoconstruct composed of a gold nanostar (AuNS) core and a ligand shell of a G-quadruplex DNA aptamer AS1411 (Apt) supporting both targeting and therapy capabilities. We examined the toxicity of the nanoconstructs (Apt-AuNS) at four different injected concentrations. At the highest dose tested (48 mg/kg), maximal tolerated dose was not reached. Clinical pathology showed no apparent signs of acute toxicity. Interestingly, the nanoconstructs circulated longer in female rats compared to male rats. In two different tumor models, the biodistribution of Apt-AuNS, especially tumor accumulation, was different. Accumulation of Apt-AuNS was 5 times higher in invasive breast cancer tumors compared to fibrosarcoma tumors. These results provide insight on identifying a tumor model and nanoconstruct for *in vivo* studies, especially when an *in vitro* therapeutic response is observed in multiple cancer cell lines.

From the Clinical Editor: This study investigated the toxicity and distribution of aptamer loaded gold nanostars in a rodent model of invasive breast cancer and fibrosarcoma. Acute toxicity was not identified even in the highest studied doses. Fivefold accumulation was demonstrated in the breast cancer model compared to the fibrosarcoma model. Studies like this are critically important in further clarifying the potential therapeutic use of these nanoconstructs, especially when ex vivo effects are clearly demonstrated.

Key words: Gold nanostars; Gold nanoconstructs; Aptamer; Toxicity; Biodistribution

Nanoparticles (NPs) are being considered as novel cancer therapeutic agents because of their ability to deliver high local concentrations of drugs to tumors.[1,2] In particular, gold nanoparticles (AuNPs) are a promising anti-cancer platform because they are biocompatible, their surfaces can be easily functionalized, and they respond to near-infrared (NIR) light.[3] When AuNP cores are surrounded by a shell of biomolecular ligands, these entities are referred to as nanoconstructs.[4-6] Nanoconstructs improve stability and tumor accumulation of drug[5,7] and also exhibit decreased toxicity by reducing non-specific uptake in healthy tissues compared to free biomolecules.[6-10] As an increased number of therapeutic nanoconstructs are being developed,[11-13] a comprehensive understanding of the biodistribution and *in vivo* toxicity is critical for a side-by-side comparison of their therapeutic window and possible side effects.[11,14] Despite numerous reports on the *in vivo* fate of bare or polyethylene glycol (PEG)-modified AuNPs,[11] only a few Au nanoconstructs conjugated with

This work was supported by National Institutes of Health Director's Pioneer Award DP1OD003899 and the H Foundation Cancer Research Fund, the Malkin Scholar Award, and the Rosenberg Award by the Robert H. Lurie Comprehensive Cancer Center at Northwestern University. We acknowledge government support under FA9550-11-C-0028 and awarded by the Department of Defense, Air Force Office of Scientific Research, National Defense Science and Engineering Graduate (NDSEG) Fellowship, 32 CFR 168a (K.S.B.C.). The Developmental Therapeutics Core at Northwestern University is partially supported by the NCI Cancer Center Support Grant 2 P30 CA060553-19. Metal analysis and organ digestion were performed at the Northwestern University Quantitative Bioelemental Imaging Center supported by National Science Foundation CHE-9810378/005 and NASA Ames Research Center NNA06CB93G. UV–vis spectroscopic measurements and immunoblotting were performed at the NU Keck Biophysics Facility supported by Cancer Center Support Grant (NCI CA060553). TEM experiments were conducted at the Biological Imaging Facility (BIF) and Northwestern University's Atomic and Nanoscale Characterization Experimental Center (NUANCE).

* Corresponding author.
E-mail address: todom@northwestern.edu (T.W. Odom).
[1] The authors contributed equally.

http://dx.doi.org/10.1016/j.nano.2014.10.005
1549-9634/

targeting biomolecules and/or drugs have been thoroughly evaluated regarding their safety and clinical potential.[15-18]

The main physicochemical factors that affect biodistribution and toxicity of nanoconstructs are size, shape, charge and surface ligands.[11,12,14] Size is a key parameter that dominates *in vivo* behavior of NPs. AuNP diameters between 10 and 200 nm primarily accumulate in organs of the mononuclear phagocyte system (MPS), especially liver and spleen,[19-21] while particles smaller than 10 nm are rapidly filtered by the kidneys and cleared by urinary excretion.[22,23] The second major characteristic is charge, which is determined by the capping ligands on the AuNP. For example, AuNPs coated with positively charged molecules such as CTAB ($\zeta = 48 \pm 2$ mV on AuNPs in water)[24] show high accumulation in all organs and exhibit severe cytotoxic effects from disruption of the cell membrane.[25,26] AuNPs with negatively charged capping molecules such as citrate ($\zeta = -33 \pm 4$ mV on AuNPs in water)[18] are prone to opsonization and also accumulate in MPS organs; however, they are much less toxic compared to positively charged AuNPs.[25,26] Neutral molecules such as PEG ($\zeta = -0.5 \pm 0.4$ mV on AuNPs in water)[27] help prevent opsonization by creating a charge shielding layer as well as steric hindrance to minimize adsorption of serum proteins.[28,29] Thus, grafting neutrally charged ligands to AuNPs can extend the plasma half-life of nanoconstructs by 3-20 times compared to negatively charged particles.[30] Recently, several studies reported that shape of AuNPs affected rate and mechanism of cellular uptake of AuNPs *in vitro* and biodistribution *in vivo*.[31,32] Although differences in biodistribution and tumor accumulation of PEGylated AuNPs of similar sizes but different shapes have been observed,[33,34] a comparison of the toxicological properties of these nanoconstructs has not been reported.

While size, shape, and charge considerations are crucial to the design of new nanoconstructs, the surface modification of NPs with functional biomolecules acting as targeting ligands and/or drugs can also play a major role in determining properties of the nanoconstructs.[35] Functional surface ligands often make prediction of the fate and toxicity of nanoconstructs more difficult, however, since *in vivo* behavior depends not only on the size and charge of the nanoconstructs but also ligand properties on the NP surface.[16,17,36] Thus, each novel nanoconstruct requires separate and thorough characterization as part of its pre-clinical evaluation.

Several studies have investigated the *in vivo* distribution and toxicity of AuNPs loaded with monoclonal antibodies (mAb) that target breast tumors overexpressing the epidermal growth factor receptor (EGFR) or human epidermal growth factor receptor 2 (HER2).[16,17] Although anti-EGFR nanoconstructs accumulated 1.5-9× higher in breast tumors than control IgG-coated constructs, the Au content in MPS organs was 2.5-5× higher compared to that in tumor, which is likely due to negatively charged surfaces created by the mAb shell.[16,17,37] One Au nanoconstruct currently in clinical trials consists of tumor necrosis factor-α (TNF-α), a protein that acts as an anti-cancer drug, grafted on PEGlyated AuNPs; this construct showed lower toxicity compared to free TNF-α.[7,15,36] Results of a phase I clinical trial reported that this nanoconstruct did not reach a maximum tolerated dose (MTD) even at concentrations exceeding three times that of the toxic dose of free TNF-α.[15] Accumulation of TNF-α-PEG-AuNPs in the tumor of prostate tumor-bearing nude mice reached up to 4% ID/g (injected dose per gram) over 72 h after a single intravenous (i.v.) injection. A large amount of Au, however, was detected in the liver and spleen of the animals (*ca.* 15-30× the Au content in tumor).[15,36] Another therapeutic Au nanoconstruct coated with PEG and *Bcl2L12* siRNA accumulated in murine intracerebral glioma tumors via the enhanced permeability and retention (EPR) effect after 5 injections (therapeutic dose = 10 mg/kg siRNA per body weight or ~180 mg/kg Au per body weight). However, Au content in the liver and spleen was *ca.* 19-30× higher than that in tumor. Toxicological evaluation in mice and rats indicated that at the therapeutic ID, there was no significant toxicity observed for the constructs.[18]

Recently, we introduced a nanoconstruct (Apt-AuNS) composed of a gold nanostar (AuNS) core and a shell of G-quadruplex aptamer AS1411 (Apt) that acts as both a tumor targeting ligand and an anti-cancer drug.[10,38] Apt-AuNS binds to the shuttle protein nucleolin (NCL) through Apt and is trafficked to the perinuclear region of cancer cells.[10,39] Interactions between the nanoconstruct and the nucleus resulted in severe deformation of the nuclear envelope, double-stranded DNA breaks in the nucleus, and ultimately, apoptosis of cancer cells.[9,10] The treatment of nanoconstructs in tandem with NIR, light-triggered release of AS1411 at the localized surface plasmon (LSP) resonance of AuNS increased the percentage of cancer cell death by 50% compared to treatment with only the nanoconstruct.[9] Importantly, NCL is one of few ubiquitous proteins that have been discovered on the surface of diverse cancer cell types.[39] We demonstrated that Apt-AuNS resulted in decreased cell viability for a 12-line cancer cell panel and showed no adverse effects on a normal cell panel.[9] To assess the potential of Apt-AuNS toward translational applications, an initial evaluation of the *in vivo* toxicity and biodistribution of Apt-AuNS is needed.

Here, we report an *in vivo* evaluation of toxicology and biodistribution of a highly anisotropic Au nanoconstruct (Apt-AuNS) having a ligand shell with both targeting and therapy capabilities. We conducted our study in three different animal models: Sprague–Dawley rats (male and female), breast-tumor bearing nude mice (female), and fibrosarcoma-tumor bearing nude mice (female). The toxicity of Apt-AuNS was evaluated at four injected doses (ID), and even at high ID up to 48 mg Au per kg bodyweight, MTD was not reached. No signs of acute toxicity were observed after complete assessment of clinical pathology including hematology and clinical chemistry. We found that the biodistribution of AuNS nanoconstructs, and especially tumor accumulation, was different in the two tumor models (fibrosarcoma and breast cancer), even though Apt-AuNS showed similar uptake and *in vitro* response in both cancer cell lines.[9] Our results confirm the importance of *in vivo* testing especially when there are multiple *in vitro* models that respond positively to the same nanoconstruct.

Methods

Synthesis and characterization of AuNS, Apt-AuNS and Apt-AuNS-PEG

AuNSs were synthesized by the reduction of gold chloride ($HAuCl_4$) in HEPES buffer at room temperature.[40] The nanoparticles typically had 2-9 branches with average tip-to-tip distances ca. 50 nm as measured by transmission electron microscopy (Figure

Table 1
Characterization of AuNS, Apt-AuNS, PEG-modified Apt-AuNS and PEG-AuNS.

Type	LSPR (nm)	Avg. hydrodynamic diameter (nm)	ζ-Potential (mV)	No. of AS1411 per AuNS	No. of PEG per AuNS
AuNS	800	45.8 ± 2.1	−26.1 ± 2.9 (Water)	–	–
Apt-AuNS	820	68.8 ± 1.8	−16.0 ± 3.0 (PBS)	110 ± 6	–
Apt-AuNS-PEG	822	68.4 ± 3.5	−9.30 ± 2.0 (PBS)	95 ± 4	1050 ± 40
PEG-AuNS	816	52.7 ± 2.2	−5.10 ± 4.0 (PBS)	–	2150 ± 60

S1). The effective hydrodynamic diameter measured by dynamic light scattering (DLS) was 46 ± 2 nm (Table 1). In water, the HEPES layer was negatively charged and resulted in an overall surface charge of $\zeta = -26 \pm 3$ mV for AuNS. We synthesized Apt-AuNS through a two-day salt-aging process after thiolated AS1411 was mixed with the AuNS suspension (Supporting information).[9,41] An increase in average hydrodynamic diameter of the nanoconstruct (70 ± 2 nm) compared to AuNS confirmed that Apt was successfully grafted on the NPs. Because phosphate buffered saline (PBS) was vehicle for i.v. (intravenous) injection of Apt-AuNS, we evaluated stability in PBS. The LSP resonance of nanoconstructs in PBS was similar to that in water at 820 nm (Figure S2), and $\zeta = -16 \pm 4$ mV. Importantly, Apt-AuNS in whole blood showed only slight broadening of the LSP, which is most likely due to protein adsorption, with the resonance peak remaining at 820 nm. Thus, the nanoconstructs appear to be stable in physiological environments (Figure S2). Quantitative analysis showed that there were *ca.* 110 AS1411 strands (55 Apt dimers) per AuNS (Supporting Information); the G-quadruplex secondary structure of AS1411 was also maintained once the aptamer was grafted on the AuNS.[10]

Because negatively charged nanoconstructs can result in high Au accumulation in the liver and spleen of the animals, for biodistribution studies with tumor models, we back-filled Apt-AuNS with PEG to yield nanoconstructs (Apt-AuNS-PEG) with a surface charge closer to neutral. Apt-AuNS-PEG were synthesized by incubating 2 kDa thiolated PEG with Apt-AuNS ([PEG]:[AuNS] 8500:1) overnight. Apt-AuNS-PEG nanoconstructs had an average hydrodynamic diameter of 68.4 ± 3.5 nm with surface charge of −9.3 ± 2.0 mV measured in PBS, which is 7 mV more positive than Apt-AuNS without PEG (Table 1). To quantify the number of PEG and AS1411 on Apt-AuNS-PEG, we synthesized nanoconstructs with Cy5-labeled Apt and FITC-labeled PEG (Supporting Information). We determined that on average there were 95 ± 4 AS1411 strands (ca. 50 Apt homodimers) and 1050 ± 40 PEG strands per AuNS. For comparison, we also synthesized PEG-AuNS constructs, which had an average hydrodynamic diameter of 52.7 ± 2.2 nm (Table 1). Full coverage of PEG on AuNS resulted in *ca.* 2150 ± 60 strands of PEG per AuNS and a nearly neutral surface charge of −5.1 ± 4.0 mV in PBS. Important for *in vivo* work, the simplicity of both the AuNS core and nanoconstruct syntheses can be easily scaled to 5 L.[9]

Toxicology of rats

To evaluate the biodistribution of Apt-AuNS in non-tumor animals, three male and three female Sprague–Dawley (Crl:SD) rats (200-220 g) were assigned to each of five test groups. Apt-AuNS or PBS was administered to the animals ($n = 6$ per group: 3 females and 3 males) by i.v. bolus injection as a single dose. The injected doses of Apt-AuNS included 0.48. 4.8, 9.6 and 48 mg of Au per kg of animal (mg/kg). Animals were checked twice after injections (a.m. and p.m.) for mortality, abnormalities, and any signs of pain or distress. Cage-side observations were conducted daily. Detailed observation was conducted on day 1 before dosing and on the day of sacrifice. Body weight was recorded before dosing, on day 2 (48 h after the injection) and on day 14. Blood samples were collected for hematology and clinical chemistry and were analyzed by Charles River Laboratories (Boston, MA). Student's t-test was performed to evaluate the significant difference among treatment groups ($p < 0.05$ was considered as a significant difference).

Tumor implantation and tail vein injection of nanoconstructs in nude mice

Nude mice, Crl:NU-Foxn1nu, were purchased from Charles River (Portage, MI) and Taconic (Hudson, NY). The animals were acclimated up to 7 days before tumor inoculation. Metastatic breast cancer cells (MDA-MB-231) and fibrosarcoma cells (HT-1080) were purchased from ATCC and maintained in RPMI 1640 media supplemented with 10% fetal bovine serum (FBS), at 5% CO_2 and 37 ° C. The cells were inoculated at a density of 3×10^6 cells subcutaneously for MDA-MB-231 and 1×10^6 cells for HT-1080. The viability of the cells was confirmed to be above 90% with passage number less than 15 at inoculation. Before inoculation, the cells were tested against human and mouse infectious diseases as guided by Northwestern Institutional Animal Care and Use Committee (IACUC). On the day of experiments, mice were grouped in separate cages ($n = 3$). The mice were anesthetized with isoflurane/oxygen. Nanoconstruct suspensions in sterile PBS were injected intravenously through the tail vein at a dose of 4.8 mg/kg for breast tumor bearing mice and 9.6 mg/kg for fibrosarcoma mice once the tumor volume average reached 100-250 mm^3. The volume of injection was adjusted to ~100 μL per 20 g of bodyweight. After the mice were euthanized, a section of each organ was digested in a mixture of nitric acid (HNO_3) and hydrochloric acid (HCl) (1:1 ratio by volume) for inductively coupled plasma–mass spectrometry (ICP-MS) analysis to determine Au content in the organs.

Results

Biodistribution and clearance of Apt-AuNS in non-tumor rats

Because drug responses are often different between female and male patients,[42] we conducted a thorough evaluation of how

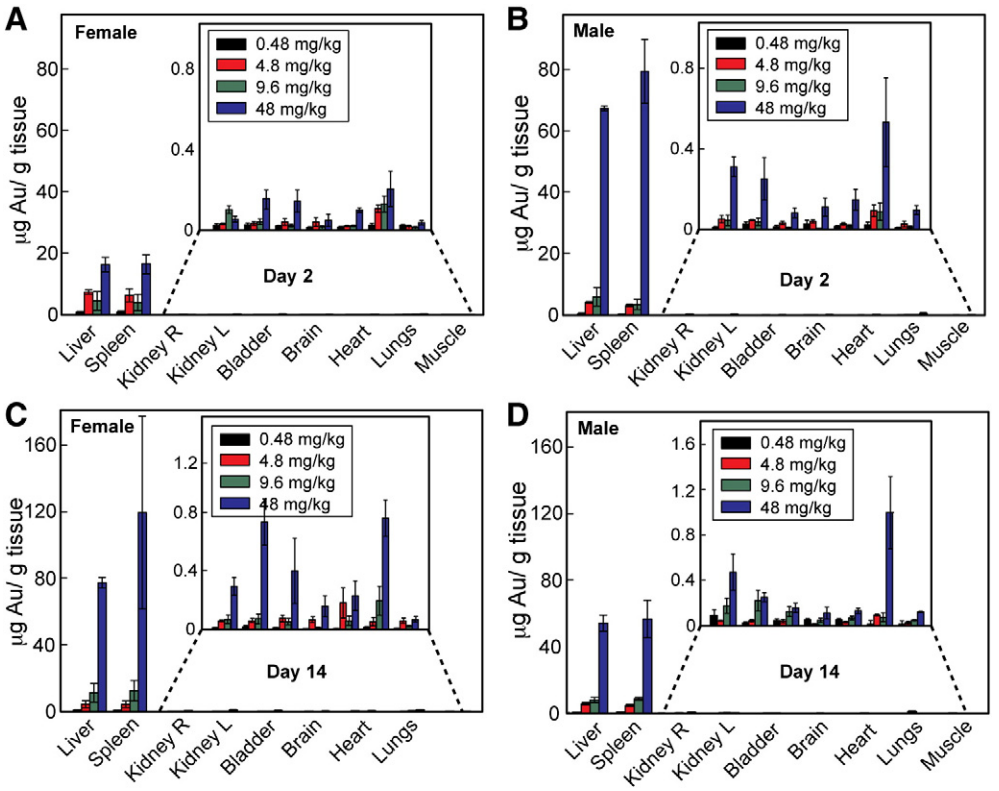

Figure 1. Biodistribution of gold nanostar nanoconstructs in female and male Sprague–Dawley rats after injection. **(A-B)** At t = 2d, the nanoconstructs mostly accumulated in the liver and spleen. As the ID increased, the Au content in all organs also increased. **(C-D)** Au accumulation in MPS organs increased significantly in female rats, while similar amounts were detected in MPS organs of male rats. For other organs, Au accumulation increased from 2 to 14 days after injection. The amount of AS1411 was estimated based on the assumption that there were 110 AS1411 per AuNS and that no DNA aptamer degraded after being grafted on the Au surface.

nanoconstructs were distributed in both genders. The range of injected dose (ID) was chosen based on the *in vitro* IC_{50} of Apt-AuNS in HeLa and MDA-MB-231, which is equivalent to 4.8 mg/kg *in vivo*.[9] After i.v. injection, the rats were sacrificed and organs collected at 2 days (t = 2d) and 14 days (t = 14d). These time points were selected based on common protocols to monitor acute toxicity.[43] Figure 1 summarizes the biodistribution of Apt-AuNS at t = 2d and t = 14d after injection. High accumulation of nanoconstructs in MPS organs (liver and spleen) was similar to that for AuNPs coated with PEG and/or functional biomolecules.[1,11] At t = 2d, Apt-AuNS were primarily found in the liver and spleen of animals at all ID, and the Au content was similar in both organs (~15 μg Au/g tissue for female rats and ~70 μg Au/g tissue for male rats at 48 mg/kg). Interestingly, we observed clear differences in the amount of Au in MPS organs between male and female rats. Two days after i.v. injection, the Au in the liver and spleen was almost 5-times lower in female rats than in male rats. This result is consistent with a gender-dependent study in mice where the half-life of Ag nanoconstructs (40 nm) was observed to be twice as long in females compared to males.[44] We found that Apt-AuNS also accumulated in lungs and kidneys, although the amounts were significantly lower (50-200×) than that in MPS organs (Figure 1). As dose increased, we also observed increases in the Au content of all organs, which suggests that accumulation of AuNS nanoconstructs in organs depends on dose. These data are important for future studies that assess the *in vivo* pharmacokinetics of the nanoconstructs.

The amount of Au in MPS organs increased significantly in female rats (from 15 μg/g of tissue to *ca*. 100 μg/g of tissue at the highest ID) from 2 days to 14 days (Figure 1, *A*, *C*), which suggests that Apt-AuNS can circulate for at least 2 days in female rats. The Au content found in MPS organs of male rats, however, decreased slightly between 2 and 14 days after injection (Figure 1, *B*, *D*), implying clearance of the nanoconstructs from these organs. To evaluate other potential clearance routes for Apt-AuNS, we measured the Au content in the kidneys and urine of all animals. Because the size of Apt-AuNS (around 70 nm) is not suitable for renal clearance, only trace amounts of Au were found in the kidneys and the bladder. The high accumulation of Au in MPS organs is consistent with the typical clearance mechanism of hydrophilic particles between 10 and 200 nm.[1,11] We also observed a small amount of Au (<0.1 μg/g) in the brain of animals, which is similar to that from PEGlyated AuNPs and another oligonucleotide-coated AuNPs.[11,18,27] Au content in the brains of both female and male rats increased slightly from *ca*. 0.02 μg/g (t = 2d) to *ca*. 0.06 μg/g (t = 14d), which indicated that the nanoconstructs can potentially be delivered to the brain.

Observation of Apt-AuNS accumulation in the liver and spleen

Using electron microscopy, we examined the localization of Apt-AuNS within MPS organs. Since Au is electron dense, AuNPs can be easily identified in transmission electron microscopy (TEM) and Z-contrast scanning transmission electron microscopy (STEM)

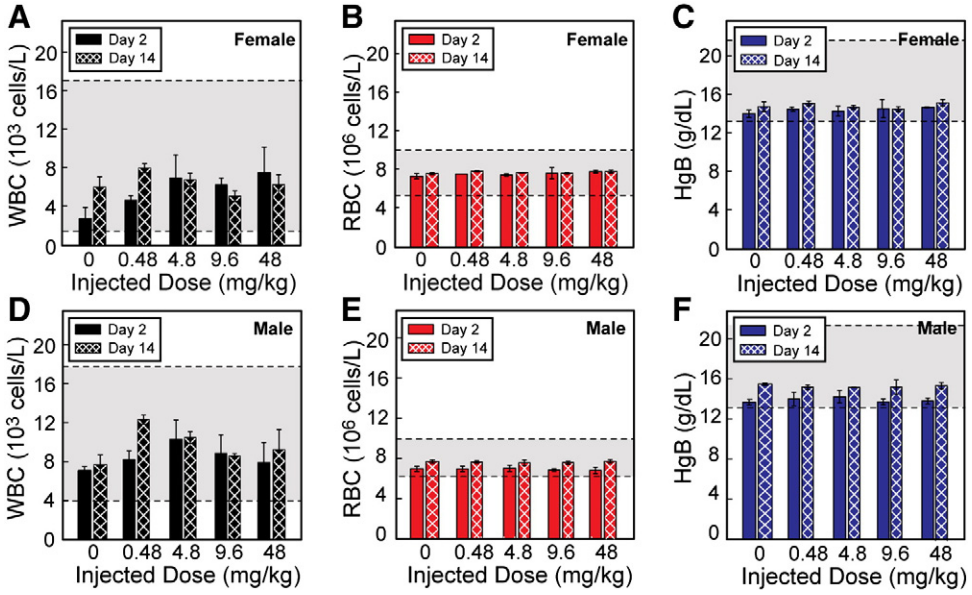

Figure 2. Hematology results in nanoconstruct treated female and male rats. At t = 2d, WBC, RBC and hemoglobin counts were within the normal range (shaded regions within dashed lines) for both **(A-C)** female and **(D-F)** male rats treated with Apt-AuNS and PBS. These hematology parameters were within the normal range for all treated animals at t = 14d.

images (Figure S3). To prepare the slices for imaging, the organs were first fixed and embedded in resin before sections (90-nm thick) were prepared (Supporting information). Characteristic Lα and M peaks of Au in the energy dispersive X-ray spectroscopy (EDS) spectra confirmed identification of Apt-AuNS in tissue sections (Figure S3). TEM images of liver revealed that Apt-AuNS were engulfed by Kupffer cells, liver macrophages whose function is to clear dead blood cells and particulates from the blood stream (Figure S4, *A-B*).[21] Kupffer cells located in the sinusoids of the liver were identified by their elongated or stellate appearance, while hepatocytes were identified by their round nuclei and large cytoplasms that contain glycogen and high number of mitochondria.[45] In the 24 liver sections that we examined, we found no particles in the hepatocytes. Furthermore, we observed no changes in the morphology of hepatocytes between the control and treated (48 mg/kg Apt-AuNS) animals. We also found Apt-AuNS in spleen cells (Figure S4, *C-D*), which is expected because the spleen also functions as a blood filter.

Effects of Apt-AuNS on hematology and clinical chemistry in rats

We used standard hematology parameters for analysis[46,47] including white blood cell (WBC), red blood cell (RBC), hematocrit (HCT), mean corpuscular volume (MCV), hemoglobin (HGB), platelet (PLT), mean corpuscular hemoglobin (MCH), and mean corpuscular hemoglobin concentration (MCHC). Figure 2 summarizes the hematology results in female and male rats after injection with Apt-AuNS or PBS. At t = 2d, the WBC count slightly increased (6.5×10^3 cell/L) in female rats treated with Apt-AuNS compared to the PBS-treated animals (3.5×10^3 cell/L) (Figure 2, *A*). All WBC counts at t = 2d for female and male rats, however, were within the normal clinical range (2.4-14.7 $\times 10^3$ cell/L, number of animals = 250) indicating no significant inflammation.[48] At t = 14d, the WBC count (5.5-12 $\times 10^3$ cell/L, $P > 0.1$) of all treated animals also suggested that there was no inflammatory response in the animals even at the highest concentrations of Apt-AuNS (48 mg/kg) (Figure 2, *C* and *D*). There were no substantial differences between injected and control groups for other hematology markers, and all were within the normal ranges (Figures 2 and S5).

Since Apt-AuNS primarily accumulated in the liver and spleen with lower Au content in the kidneys, we analyzed biomarkers that represented potential acute toxicity in these organs. We focused specifically on the enzymes alanine aminotransferase (ALT), aspartate aminotransferase (AST), and blood urea nitrogen and creatinine ratio (BUN/CREA), since elevated levels of these indicators are closely related to liver and kidney damage.[49] In addition, we conducted a full standard blood chemistry analysis including albumin (ALB), alkaline phosphatase (ALK), total bilirubin (TBIL), total protein (TP), calcium (CA), cholesterol (CHOL), glucose (GLU), inorganic phosphate (PHOS), triglycerides (TRIG), high-density lipoprotein (HDL), and low-density lipoprotein (LDL).[48] The biochemistry results indicated that levels of ALT and AST in all treated groups were within the normal range at t = 2d and t = 14d with no statistically significant differences ($P > 0.1$) (Figure 3). Also, we analyzed the BUN/CREA ratio in the serum, which is an important indicator of kidney function. The ratios were within the normal range in all animals treated with various dosages of Apt-AuNS and PBS, and there was no abnormality in the kidney function (Figure 3). Our analyses of other hematologic and biochemistry indicators showed no difference between the Apt-AuNS injected animals and the PBS control group (Figure S6). Pathology results also showed that there was no structural alteration or abnormality in the liver and spleen between PBS (vehicle control) treated and Apt-AuNS treated rats at all injected concentrations (Figure 4). Gross organ and pathological examination also showed no structural changes and further confirmed no sign of toxicity in all organs (Figure S7).

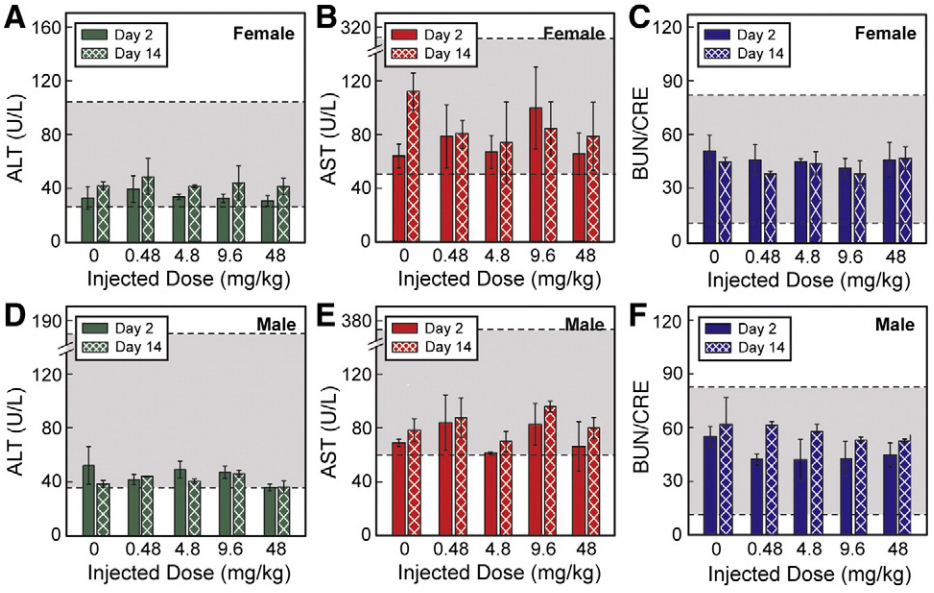

Figure 3. Clinical pathology analysis in nanoconstruct-treated rats. At t = 2d, the clinical pathology results indicated no significant differences between the **(A-C)** female and **(D-F)** male nanoconstruct-injected rats and their PBS treated group. AST and ALT levels and BUN/CRE ratios were within the normal range (shaded regions within dashed lines) indicating that no malfunction in the livers and kidneys of the animals. No signs of acute toxicity were observed at t = 14d.

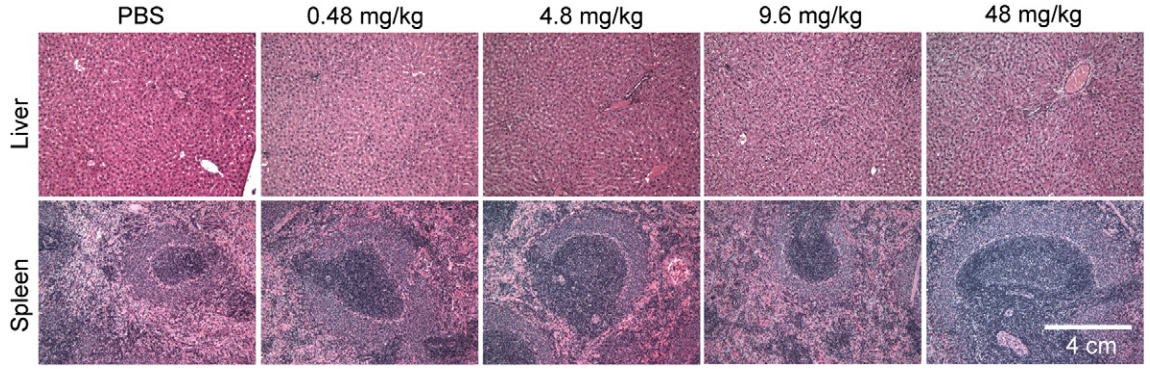

Figure 4. Pathology sections of liver and spleen in Apt-AuNS treated animals. No structural alteration or abnormality was observed in any organ treated with PBS or Apt-AuNS at all ID.

Accumulation of Apt-AuNS in tumor-bearing mice

Since AuNS loaded with targeting and therapeutic AS1411 did not show acute toxicity at high ID up to 48 mg/kg of nanoconstruct, we investigated how the nanoconstruct behaved in tumor-bearing mice models. We examined biodistribution of nanoconstructs and/or PEGylated nanoconstructs in two tumor-bearing mice models: fibrosarcoma and breast cancer. We chose to study these two tumor models since they present near the skin surface and are amenable to light-triggered drug release treatment. In addition, we demonstrated that HT-1080 fibrosarcoma and MDA-MB-231 metastatic breast cancer cells overexpress surface and cytoplasmic NCL and are susceptible to Apt-AuNS *in vitro*.[9] We first inoculated HT-1080 or MDA-MB-231 cells on the right flank of female nude mice, and tumors were grown for two weeks up to 10 mm in diameter. The mice were then administered a single dose of 4.8 mg/kg of

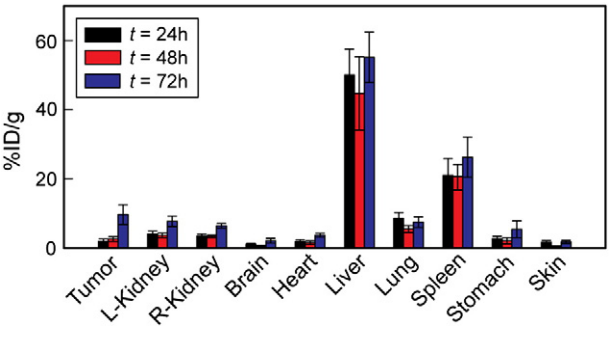

Figure 5. Biodistribution of Apt-AuNS in breast-tumor bearing mice. Accumulation reached 10% ID/g in tumor 72-h after injection. Apt-AuNS showed high accumulation in the liver and spleen with no significant increase from 24 h to 72 h after injection.

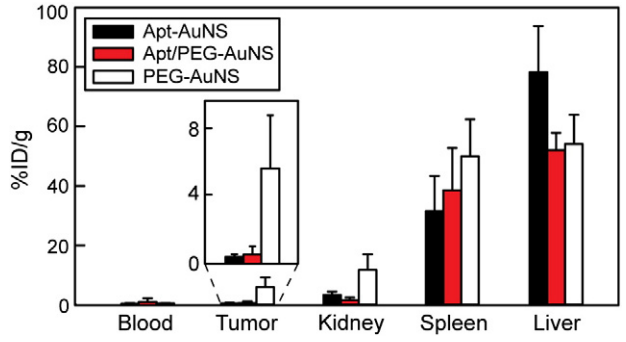

Figure 6. Biodistribution of PEG-modified and -unmodified AuNS nanoconstructs in fibrosarcoma tumor-bearing mice. A significant decrease of PEG-modified nanoconstruct in the liver compared to Apt-AuNS without PEG was observed.

nanoconstruct or PBS via i.v. injection for the breast cancer model and 9.6 mg/kg of nanoconstruct or PBS for the fibrosarcoma model. These concentrations were chosen because they can be well tolerated by the animals and show *in vitro* therapeutic responses in MDA-MB-231 and HT-1080 cells.[9,41] The mice were sacrificed at 24, 48 and 72 h after injection for breast tumor-bearing mice and at 24 h after injection for fibrosarcoma-bearing mice.

First, we characterized the biodistribution of Apt-AuNS constructs in the breast tumor models. Forty-eight hours after i.v. injection of 4.8 mg/kg, accumulation of the nanoconstructs in the liver was not statistically different between tumor-bearing mice (44 ± 11 %ID/g) and non-tumor rats (51 ± 21 %ID/g) (Figures 5 and S8). The Au content in the liver and spleen did not change from $t = 24$ h (50 ± 7 %ID/g for liver and 21 ± 5 %ID/g for spleen) to $t = 72$ h (57 ± 8 % for liver and 24 ± 6 % for spleen) in breast-tumor bearing mice (Figure 5). At $t = 24$ h, we observed 2 ± 0.5% ID/g Apt-AuNS in the breast tumor, which increased to 9.7 ± 2.4% at $t = 72$ h. Increased accumulation of nanoconstruct in the tumors from 24 h to 72 h indicated that Apt-AuNS could circulate for longer than 24 h. We also found Au content in kidneys, which increased from 3.5 ± 0.7% ID/g at $t = 24$ h to 7.5 ± 1.3% ID/g at $t = 72$ h. Similarly, there were slight increases in Au content in other organs from $t = 24$ h to $t = 72$ h except for lung, which decreased from 8.6% to 7.5%, although the difference is not statistically significant ($P > 0.1$) (Figure 5).

To understand whether Apt-AuNS would behave differently in a different tumor model, we investigated its distribution in fibrosarcoma-bearing nude mice. Figure 6 shows that the %ID/g of Au in the livers of fibrosarcoma-bearing mice was higher than that in the breast-tumor model at 24 h after injection (80 ± 16 %ID/g compared to 50% ± 7 %ID/g). Accumulation in spleen and kidneys, however, appeared to be similar in both tumor-bearing models (~25 %ID/g in spleen and ~4%ID/g in kidneys) (Figures 5 and 6). Interestingly, while higher *in vitro* uptake of Apt-AuNS was observed in HT-1080 cells compared to MDA-MB-231 cells,[9] we found a much lower Au content in fibrosarcoma tumors (0.4 ± 0.2 %ID/g) compared to that in breast tumors (2 %ID/g) at $t = 24$ h (Figures 5 and 6).

Since relatively poor tumor accumulation of Apt-AuNS was achieved in fibrosarcoma tumor models, we tested whether incorporating PEG onto the Apt-AuNS could improve tumor uptake. A single injection of 9.6 mg/kg of Apt-AuNS-PEG and PEG-AuNS was delivered to fibrosarcoma-bearing nude mice, and biodistribution of the nanoconstructs was evaluated 24 h after injection. While the %ID/g in the spleen was not significantly different among Apt-AuNS-PEG, PEG-AuNS and the original Apt-AuNS, there was a reduction of Au accumulation in the liver of mice treated with Apt-AuNS-PEG (52 ± 5.8 %ID/g) and PEG-AuNS (53 ± 7 %ID/g) compared to those treated with Apt-AuNS (~80 %ID/g) (Figure 6). We also observed a decrease in Au content in the kidneys of Apt-AuNS-PEG treated mice (1.5 ± 0.9 %ID/g) compared to Apt-AuNS treated mice (3.5 %ID/g). A higher amount of Au in the kidneys (12 ± 5.3 %ID/g), however, was detected in mice treated with PEG-AuNS. These results were surprising and require further investigation, since the average diameter of PEG-AuNS (~48 nm) is much larger than the average particle size for renal clearance (<10 nm). Unfortunately, there was no statistical difference in uptake of Apt-AuNS-PEG (0.6 ± 0.5 %ID/g) and Apt-AuNS (0.4 ± 0.2 %ID/g) in the tumor after 24 h, but PEG-AuNS accumulated in tumor at 6 ± 3 %ID/g (Figure 6).

Discussion

We found that Apt-AuNS nanoconstructs do not cause acute *in vivo* toxicity even at the highest injected dose of 48 mg/kg. The distribution of nanoconstructs in non-tumor bearing rats showed accumulation in MPS organs as expected since the overall surface charge was negative (−16 mV in PBS). Our data showed that even though the nanoconstructs accumulated in the liver at high concentrations, there were no apparent signs of toxicity. We expect that the lack of acute toxicity in the liver of the rats can be attributed to high accumulation in the macrophages instead of the hepatocytes.

A direct comparison of the two tumor models in our study suggests that Apt-AuNS accumulated more in the liver of fibrosarcoma mice compared to that of breast-cancer mice, but a 5× higher content of Au could be found in breast compared to fibrosarcoma tumors. This difference in Apt-AuNS accumulation in these two tumors may possibly be attributed to differences in angiogenesis, and more likely necrosis of the two tumor types since MDA-MB-231 tumors contain 80-90% necrotic regions, which are often abundant with macrophages.[50] These results also support previous claims that nanoconstructs with impressive *in vitro* performances may not be the best candidate for therapeutic studies.[29] Thus, *in vivo* evaluations of different formulations and tumor targets are critical to evaluate the clinical relevance of nanoconstructs for therapeutics.

We attribute the lower accumulation of Apt-AuNS-PEG compared to PEG-AuNS in tumor to incomplete surface coverage of PEG on Apt-AuNS. The partial coverage (*ca.* 1100 PEG per Apt-AuNS-PEG) only increased the surface charge of the nanoconstruct to *ca.* −10 mV; the full coverage of PEG on AuNS (*ca.* 2200 PEG per PEG-AuNS) resulted in almost neutral surface charge (Table 1). Because of the PEG-only layer, the neutrally charged nanoconstructs could avoid macrophage engulfing and reach the vasculature of the tumor more readily than Apt-PEG-AuNS. However, we hypothesize that once the targeted constructs

are taken up by tumors, Apt-PEG-AuNS would be more likely to penetrate cancer cells compared to PEG-AuNS due to the nucleolin targeting capabilities of AS1411. Our next investigations will focus on optimizing both AS1411 loading density and PEG surface coverage to maximize delivery to tumors as well as deliver localized therapeutic doses of AS1411.

In conclusion, we have demonstrated that Apt-AuNS is a biocompatible nanoconstruct that causes no *in vivo* acute toxicity. There were no signs of abnormality observed in any of the organs of non-tumor rats at all injected dosages. We also found that significant uptake in the tumor (up to 10 %ID/g) can be obtained 72-h after injection. Our results also indicated that adding PEG to the nanoconstruct surface could reduce accumulation in the liver. Importantly, Apt-AuNS showed tumor accumulation that was higher in breast-tumor bearing mice compared to fibrosarcoma-bearing mice. We anticipate that these results may provide important information on selecting a suitable tumor model and nanoconstruct system for *in vivo* studies, especially when an *in vitro* therapeutic response is observed in multiple cancer cell lines.

Appendix A. Supplementary data

Supplementary data to this article can be found online at http://dx.doi.org/10.1016/j.nano.2014.10.005.

References

1. Dykman LA, Khlebtsov NG. Uptake of engineered gold nanoparticles into mammalian cells. *Chem Rev* 2014;**114**:1258-88.
2. Wang AZ, Langer R, Farokhzad OC. Nanoparticle delivery of cancer drugs. *Annu Rev Med* 2012;**63**:185-98.
3. Xie J, Lee S, Chen X. Nanoparticle-based theranostic agents. *Adv Drug Deliv Rev* 2010;**62**:1064-79.
4. Ferrari M. Cancer nanotechnology: opportunities and challenges. *Nat Rev Cancer* 2005;**5**:161-71.
5. Cuenca AG, Jiang H, Hochwald SN, Delano M, Cance WG, Grobmyer SR. Emerging implications of nanotechnology on cancer diagnostics and therapeutics. *Cancer* 2006;**107**:459-66.
6. Yezhelyev MV, Gao X, Xing Y, Al-Hajj A, Nie S, O'Regan RM. Emerging use of nanoparticles in diagnosis and treatment of breast cancer. *Lancet Oncol* 2006;**7**:657-67.
7. Paciotti GF, Myer L, Weinreich D, Goia D, Pavel N, McLaughlin RE, et al. Colloidal gold: a novel nanoparticle vector for tumor directed drug delivery. *Drug Deliv* 2004;**11**:169-83.
8. Dobrovolskaia MA, McNeil SE. Immunological properties of engineered nanomaterials. *Nat Nanotechnol* 2007;**2**:469-78.
9. Dam DH, Culver KS, Odom TW. Grafting aptamers onto gold nanostars increases in vitro efficacy in a wide range of cancer cell types. *Mol Pharm* 2014;**11**:580-7.
10. Dam DH, Lee JH, Sisco PN, Co DT, Zhang M, Wasielewski MR, et al. Direct observation of nanoparticle-cancer cell nucleus interactions. *ACS Nano* 2012;**6**:3318-26.
11. Khlebtsov N, Dykman L. Biodistribution and toxicity of engineered gold nanoparticles: a review of in vitro and in vivo studies. *Chem Soc Rev* 2011;**40**:1647-71.
12. Oberdorster G, Oberdorster E, Oberdorster J. Concepts of nanoparticle dose metric and response metric. *Environ Health Perspect* 2007;**115**:A290.
13. Lewinski N, Colvin V, Drezek R. Cytotoxicity of nanoparticles. *Small* 2008;**4**:26-49.
14. Fadeel B, Garcia-Bennett AE. Better safe than sorry: understanding the toxicological properties of inorganic nanoparticles manufactured for biomedical applications. *Adv Drug Deliv Rev* 2010;**62**:362-74.
15. Libutti SK, Paciotti GF, Byrnes AA, Alexander HR, Gannon WE, Walker M, et al. Phase I and pharmacokinetic studies of CYT-6091, a novel pegylated colloidal gold-rhTNF nanomedicine. *Clin Cancer Res* 2010;**16**:6139-49.
16. Melancon MP, Lu W, Yang Z, Zhang R, Cheng Z, Elliot AM, et al. In vitro and in vivo targeting of hollow gold nanoshells directed at epidermal growth factor receptor for photothermal ablation therapy. *Mol Cancer Ther* 2008;**7**:1730-9.
17. Qian X, Peng XH, Ansari DO, Yin-Goen Q, Chen GZ, Shin DM, et al. In vivo tumor targeting and spectroscopic detection with surface-enhanced Raman nanoparticle tags. *Nat Biotechnol* 2008;**26**:83-90.
18. Jensen SA, Day ES, Ko CH, Hurley LA, Luciano JP, Kouri FM, et al. Spherical nucleic acid nanoparticle conjugates as an RNAi-based therapy for glioblastoma. *Sci Transl Med* 2013;**5**:209-20.
19. Bergen JM, Von Recum HA, Goodman TT, Massey AP, Pun SH. Gold nanoparticles as a versatile platform for optimizing physicochemical parameters for targeted drug delivery. *Macromol Biosci* 2006;**6**:506-16.
20. Diagaradjane P, Shetty A, Wang JC, Elliott AM, Schwartz J, Shentu S, et al. Modulation of in vivo tumor radiation response via gold nanoshell-mediated vascular-focused hyperthermia: characterizing an integrated antihypoxic and localized vascular disrupting targeting strategy. *Nano Lett* 2008;**8**:1492-500.
21. Sadauskas E, Wallin H, Stoltenberg M, Vogel U, Doering P, Larsen A, et al. Kupffer cells are central in the removal of nanoparticles from the organism. *Part Fibre Toxicol* 2007;**4**:10-7.
22. Semmler-Behnke M, Kreyling WG, Lipka J, Fertsch S, Wenk A, Takenaka S, et al. Biodistribution of 1.4-and 18-nm gold particles in rats. *Small* 2008;**4**:2108-11.
23. Hillyer JF, Albrecht RM. Gastrointestinal persorption and tissue distribution of differently sized colloidal gold nanoparticles. *J Pharm Sci* 2001;**90**:1927-36.
24. Parab HJ, Chen HM, Lai TC, Huang JH, Chen PH, Liu RS, et al. Biosensing, cytotoxicity, and cellular uptake studies of surface-modified gold nanorods. *J Phys Chem C* 2009;**113**:7574-8.
25. Arvizo RR, Miranda OR, Moyano DF, Walden CA, Giri K, Bhattacharya R, et al. Modulating pharmacokinetics, tumor uptake and biodistribution by engineered nanoparticles. *PLoS One* 2011;**6**.
26. Hirn S, Semmler-Behnke M, Schleh C, Wenk A, Lipka J, Schaffler M, et al. Particle size-dependent and surface charge-dependent biodistribution of gold nanoparticles after intravenous administration. *Eur J Pharm Biopharm* 2011;**77**:407-16.
27. Niidome T, Yamagata M, Okamoto Y, Akiyama Y, Takahashi H, Kawano T, et al. PEG-modified gold nanorods with a stealth character for in vivo applications. *J Control Release* 2006;**114**:343-7.
28. Alkilany AM, Shatanawi A, Kurtz T, Caldwell RB, Caldwell RW. Toxicity and cellular uptake of gold nanorods in vascular endothelium and smooth muscles of isolated rat blood vessel: importance of surface modification. *Small* 2012;**8**:1270-8.
29. Qhattal HS, Hye T, Alali A, Liu X. Hyaluronan polymer length, grafting density, and surface poly(ethylene glycol) coating influence in vivo circulation and tumor targeting of hyaluronan-grafted liposomes. *ACS Nano* 2014;**8**:523-40.
30. Kadam RS, Bourne DW, Kompella UB. Nano-advantage in enhanced drug delivery with biodegradable nanoparticles: contribution of reduced clearance. *Drug Metab Dispos* 2012;**40**:1380-8.
31. Chithrani BD, Ghazani AA, Chan WCW. Determining the size and shape dependence of gold nanoparticle uptake into mammalian cells. *Nano Lett* 2006;**6**:662-8.
32. Albanese A, Tang PS, Chan WCW. The effect of nanoparticle size, shape, and surface chemistry on biological systems. *Annu Rev Biomed Eng* 2012;**14**:1-16.
33. Black KC, Wang Y, Luehmann HP, Cai X, Xing W, Pang B, et al. Radioactive 198Au-doped nanostructures with different shapes for in vivo analyses of their biodistribution, tumor uptake, and intratumoral distribution. *ACS Nano* 2014;**8**:4385-94.

34. Chen H, Zhang X, Dai S, Ma Y, Cui S, Achilefu S, et al. Multifunctional gold nanostar conjugates for tumor imaging and combined photothermal and chemo-therapy. *Theranostics* 2013;**3**:633-49.
35. Verma A, Stellacci F. Effect of surface properties on nanoparticle–cell interactions. *Small* 2010;**6**:12-21.
36. Goel R, Shah N, Visaria R, Paciotti GF, Bischof JC. Biodistribution of TNF-alpha-coated gold nanoparticles in an in vivo model system. *Nanomedicine* 2009;**4**:401-10.
37. Bardhan R, Chen W, Bartels M, Perez-Torres C, Botero MF, McAninch RW, et al. Tracking of multimodal therapeutic nanocomplexes targeting breast cancer in vivo. *Nano Lett* 2010;**10**:4920-8.
38. Dam DH, Culver KS, Sisco PN, Odom TW. Shining light on nuclear-targeted therapy using gold nanostar constructs. *Ther Deliv* 2012;**3**:1263-7.
39. Soundararajan S, Wang L, Sridharan V, Chen WW, Courtenay-Luck N, Jones D, et al. Plasma membrane nucleolin is a receptor for the anticancer aptamer AS1411 in MV4-11 leukemia cells. *Mol Pharmacol* 2009;**76**:984-91.
40. Xie JP, Lee JY, Wang DIC. Seedless, surfactantless, high-yield synthesis of branched gold nanocrystals in HEPES buffer solution. *Chem Mater* 2007;**19**:2823-30.
41. Dam DHM, Lee RC, Odom TW. Improved in vitro efficacy of gold nanoconstructs by increased loading of G-quadruplex aptamer. *Nano Lett* 2014;**14**:2843-8.
42. Whitley H, Lindsey W. Sex-based differences in drug activity. *Am Fam Physician* 2009;**80**:1254-8.
43. Trotti A, Byhardt R, Stetz J, Gwede C, Corn B, Fu K, et al. Common toxicity criteria: version 2.0. An improved reference for grading the acute effects of cancer treatment: impact on radiotherapy. *Int J Radiat Oncol Biol Phys* 2000;**47**:13-47.
44. Xue Y, Zhang S, Huang Y, Zhang T, Liu X, Hu Y, et al. Acute toxic effects and gender-related biokinetics of silver nanoparticles following an intravenous injection in mice. *J Appl Toxicol* 2012;**32**:890-9.
45. Cross PC, Mercer KL. *Cell and tissue ultrastructure a functional perspective*. 2nd ed. W.H, Freeman; 1993420.
46. Simpson CA, Salleng KJ, Cliffel DE, Feldheim DL. In vivo toxicity, biodistribution, and clearance of glutathione-coated gold nanoparticles. *Nanomedicine* 2013;**9**:257-63.
47. Chen YS, Hung YC, Liau I, Huang GS. Assessment of the in vivo toxicity of gold nanoparticles. *Nanoscale Res Lett* 2009;**4**:858-64.
48. Derekanko MJ, Auletta CS. *Handbook of toxicology*. 3rd ed. CRC Press; 2014.
49. Types of blood tests. http://www.nhlbi.nih.gov/health/health-topics/topics/bdt/types.html.
50. Olmeda D, Moreno-Bueno G, Flores JM, Fabra A, Portillo F, Cano A. SNAI1 is required for tumor growth and lymph node metastasis of human breast carcinoma MDA-MB-231 cells. *Cancer Res* 2007;**67**:11721-31.